Paper:
Mohamed, S., Coccarelli, A., Mauro, A., Massarotti, N., Romano, M., Romano, V. & Nithiarasu, P. (2019). A novel numerical modelling approach for keratoplasty eye procedure. *Biomechanics and Modeling in Mechanobiology*
http://dx.doi.org/10.1007/s10237-019-01156-y

A novel numerical modelling approach for keratoplasty eye procedure

Salahudeen Mohamed[1], Alberto Coccarelli[2], Alessandro Mauro[1], Nicola Massarotti[1], Mario R. Romano[3], Vito Romano[4,5], Perumal Nithiarasu[2]

[1]Dipartimento di Ingegneria, Università degli Studi di Napoli "Parthenope", Isola C4, Centro Direzionale di Napoli, 80143 Napoli, Italy

[2]Zienkiewicz Centre for Computational Engineering, College of Engineering, Swansea University, Swansea SA2 8PP, UK.

[3]Department of Biomedical Sciences, Humanitas University, Via A. Manzoni 113, 20089, Rozzano (Milano), Italy.

[4]Department of Eye and Vision Science, Institute of Ageing and Chronic Disease, University of Liverpool, Liverpool, UK.

[5]Instituto Universitario Fernandez-Vega, Universidad de Oviedo and Fundacion de Investigacion on Oftalmologica, Oviedo, Spain

Corresponding author:
Dr. Salahudeen MOHAMED
Dipartimento di Ingegneria, Università degli Studi di Napoli "Parthenope", Isola C4,
Centro Direzionale di Napoli, 80143 Napoli, Italy
e-mail: salahudeen.mohamed@uniparthenope.it
Ph. 0039 3314486285

Total number of words: 3583

Number of words in abstract: 167

Number of figures: 9

Number of tables: 1

Abstract

Objective of the work is to investigate the stress and strain fields that corneal tissue and donor graft undergo during endothelial keratoplasty. In order to attach the donor graft to the cornea, different air bubble pressure profiles acting on the graft are considered. This study is carried out by employing a three-dimensional non-linear finite element (FE) methodology, combined with a contact algorithm. The ocular tissues are treated as isotropic, hyper-elastic and incompressible materials. The contact algorithm, based on the penalty-based node-to-surface approach, is used to model the donor graft-corneal interface region. The proposed computational methodology is tested against benchmark data for bending of the plates over a cylinder. The influence of geometrical and material parameters of the graft on the corneal contact-structural response is investigated. The results are presented in terms of Von Mises (VM) stress intensity, displacement and mean contact force. Results clearly indicate that the air bubble pressure plays a key role in the corneal stress and strain, as well as graft stiffness and thickness.

Keywords: Keratoplasty; Cornea transplantation; Biomechanics; Hyper-elastic model; Finite element; Contact mechanics

Nomenclature

$\mathbf{d}$	=	Displacement vector (mm)
$\boldsymbol{e}$	=	Tangent vector
E	=	Young's Modulus (Pa)
$\boldsymbol{F}$	=	Deformation gradient
f	=	Contact force (N)
$\boldsymbol{g}_i$	=	Gap vector (mm)

$\boldsymbol{N}$ = Normal vector

$\mathbf{K}$ = Stiffness matrix

$\mathbf{K_c}$ = Contact stiffness matrix

P = Bubble pressure (Pa)

$\mathbf{R_C}$ = Residual contact forces vector (N)

$\mathbf{S}$ = Internal forces vector (N)

$\mathbf{T}$ = External forces vector (N)

$\mathbf{t}$ = Traction vector (Pa)

$\boldsymbol{w}$ = dual basis vector

Greek symbols

υ = Poisson ratio

ε = penalty parameter (N/mm)

ρ = density (kg/m^3)

κ = Penalty number (Pa)

μ = Shear modulus (Pa)

$\boldsymbol{\sigma}$ = Cauchy Stress Tensor (Pa)

$\boldsymbol{\Psi}$ = Strain Energy function (Pa)

49 *Acronyms*

AC = Anterior Chamber

DM = Descemet's Membrane

VM = Von Mises

Subscripts

p = Projection

s = slave node

max = Maximum

1. Introduction

Corneal transplantation, known as keratoplasty, is a surgical procedure aiming to replace damaged cornea with healthy donor tissue. It can be used to improve sight, relieve pain and treat severe uncontrolled corneal infection [Tan et al., 2012]. In conventional surgical procedures for corneal transplantation, known as Penetrating Keratoplasty (PK), the whole cornea tissue is replaced with donor tissue. However, with the advent of sophisticated techniques, like Descemet's Stripping Automated Endothelial Keratoplasty (DSAEK) and Descemet's Membrane Automated Endothelial Keratoplasty (DMAEK), selective removal of posterior corneal tissue has achieved a decrease in post-operative complications and improved vision [Stuart et al., 2018; Parekh et al., 2018; Parekh et al., 2018].

Both DSAEK and DMAEK surgical techniques involve two steps: in the first step, partial removal of the damaged corneal basement layer, mainly the Descemet's Membrane (DM), is carried out while in the second step, a healthy donor DM is replaced. The thickness of the donor DM is selected by the surgeon based on the intensity of the damage on the host membrane. The donor DM, often referred to as graft, is inserted in the Anterior Chamber (AC) of the eye by means of scleral incision, and attached to the posterior cornea with a surgical device. Attaching the graft by a device may damage both corneal tissues and graft. For this reason, the pressure needed to attach the graft is imposed by means of an air bubbling technique as shown in Figure 1. In this technique, an air bubble is placed at the anterior part of the graft inside the Anterior Chamber (AC) of the eye and subsequently the bubble size is increased along with the pressure in order to move the graft towards the corneal basement side. This technique provides approximately 90% success rate of correct attachment of the graft to the posterior cornea, and generally it avoids further surgical device interventions with ocular tissues and corneal sutures [Stuart et al., 2018; Parekh et al., 2018; Parekh et al., 2018]. In unsuccessful cases, graft detachment may be associated with the presence of interfacial fluid between graft and cornea, but the underlying cause of these detachments is still unknown.

The employment of mathematical eye models and engineering approach in biomedical applications has proven to be a success in terms of prediction of physical quantities of interest like velocity, pressure, stress and temperature, such as for the design of biomedical equipment [Mauro et al., 2018; Mauro et al., 2018; Mauro et al., 2018; Mauro et al., 2018]. The high number of recent studies on modelling cornea biomechanics indicates a growing interest in the field [Canovetti et al., 2018; Fraldi et al., 2011; Nguyen et al., 2011; Pandolfi et al., 2006]. In the study by Studer et al., the collagen fibre distribution in a human cornea is studied using a biomechanical model, accounting for age related differences. Their results show an increase in collagen cross-linking in cornea for older age groups [Studer et al., 2010]. A finite element methodology was proposed by Lago et al. to present the in vivo characterization of biomechanical behaviour of the cornea [Lago et al., 2010]. In the numerical study by Whiteford et al., a finite element model was proposed to analyse the anisotropic behaviour of the cornea [Whitford et al., 2015]. In their study, model parameters were calibrated with the experimental data for different age-groups. Montanino et al. developed a model for analysing the air puff test on the cornea, in order to study the effect of aqueous humour on corneal deformation [Montanino et al., 2018]. In their study the influence of material and geometrical parameters on corneal deformation was also investigated.

There are no studies concerning the numerical modelling of keratoplasty, with a realistic reproduction of the corneal transplantation into a three-dimensional cornea model. Therefore, the present work represents the first attempt to theoretically describe the second step of endothelial keratoplasty procedure, i.e., the attachment of donor graft with cornea driven by air bubble pressure, in order to characterize the structural interaction between graft and cornea. This will ultimately provide insights on the design of corneal transplantation surgery, with consequent reduction of post-operative complications.

The paper is organized as follows: the next section presents the computational domain, boundary conditions, governing equations and contact mechanics algorithm. The third section first reports the numerical method validation, and then comments the results obtained from endothelial keratoplasty simulations. Finally, concluding remarks are drawn in the last section.

2. Mathematical model and numerical procedure

2.1. Computational domain and boundary conditions

The computational domains of the graft (slave body) and cornea (master body) are represented in Figure 2. The graft considered in this work is 8 mm in diameter and 120 µm in thickness [Moshirfar et al., 2014; Gormsen et al., 2018]. The cornea is assumed to have a uniform thickness equal to 520 µm, with an anterior chamber height of 15 mm. During the endothelial keratoplasty, the slave surface (pink colour in Figure 2 (top)) of graft attaches with master surface (red colour in Figure 2 (bottom)) of the cornea. Linear hexahedron elements are used to discretise the computational domain of graft and cornea with 324 and 968 elements, respectively.

In order to reproduce the air bubble pressure a space and time varying load P=P(x, z, t) is applied along the 'y' direction, normal at anterior surface (load surface) of the graft. A parabolic profile is used to describe its spatial variation, and its magnitude is gradually increased until attachment occurs, with P_{max} as the maximum value at the centre of the graft. For the cornea a fixed boundary condition (fixed b.c) is also imposed at the circumferential sides (blue colour in Figure 2). Free boundary condition is imposed at the remaining surfaces.

With regard to the cornea, the Young's Modulus and Poisson ratio υ are equal to E = 1.0 MPa and 0.4, respectively [Shih et al., 2017]. For the graft, material properties are similar to DM. However, the stiffness of the donor graft is slightly higher than the actual DM, due to the chemical treatment performed prior to the endothelial keratoplasty procedure [Last et al., 2009]. Therefore, different Young's Modulus values between 0.1 MPa and 0.3 MPa are considered in this study (Poisson ratio is maintained equal to 0.4). The Young's Modulus values of cornea and graft are experimentally measured values which are obtained from the previous studies [Shih et al., 2017, Last et al., 2009). A density ρ = 1000 kg/m^3 is assumed for both bodies. Since the study focuses on the biomechanical behaviour of cornea and graft, the presence of aqueous humor at the anterior chamber is, for sake of simplicity, not accounted for.

2.2. Governing equations and discretization

Cornea and graft are modelled as isotropic, hyper-elastic and nearly-incompressible materials [Sinha et al., 2009; Khan et al., 2016]. Finite strain theory is used for describing the kinematics of both bodies. The reference (stress free) and deformed configurations are indicated with Ω_o and Ω, respectively, and the corresponding coordinates as $X \in \Omega_o$ and $x \in \Omega$. The deformation gradient is denoted as $F = \dfrac{\partial x}{\partial X}$, whilst $J = \det F > 0$ is the local volume ratio and $\overline{F} = J^{-\frac{1}{2}} F$ is the distorsional component of the deformation gradient. The right-Cauchy deformation gradient and its isochoric counterpart are therefore defined as $C = F^T F$ and $\overline{C} = \overline{F}^T \overline{F}$ respectively. For a material which is assumed to be nearly-incompressible, the strain energy function (ψ) can be decoupled as in [Holzapfel et al., 2000]

$$\psi = \overline{\psi}(\overline{C}) + U(J) \quad , \qquad (1)$$

where $\overline{\psi}$ and U are the purely isochoric and volumetric contributions to ψ, respectively. In the current study a neo-Hookean type material has been adopted, ie,

$$\overline{\psi}(\overline{C}) = \frac{\mu}{2}(\overline{I}_1 - 3), \qquad (2)$$

in which μ is the shear modulus, $\overline{I}_1$ is the first invariant of $\overline{C}$. The volumetric component of the strain energy function is

$$U(J) = \kappa \frac{(J-1)^2}{2} \qquad (3)$$

where κ is the penalty parameter used for enforcing incompressibility.

In a standard Lagrangian description, the balance of linear momentum for an infinitesimal solid volume $d\Omega$ may be written as

$$\rho \ddot{d} - \nabla \cdot \sigma = 0, \qquad (4)$$

in which ρ is the current density, the vector $\boldsymbol{d}$ is the displacement field whereas $\boldsymbol{\sigma}$ is the second order Cauchy stress tensor. The application of the virtual work principle to the momentum conservation equation leads, after integration by parts, to

$$\int_{\Omega} \delta\mathbf{d}^{\mathrm{T}} \rho \ddot{\mathbf{d}}\, \mathrm{d}\Omega + \int_{\Omega} \delta\varepsilon^{T} \sigma \mathrm{d}\Omega - \int_{\Gamma} \delta\mathbf{d}^{\mathrm{T}} \mathbf{t} \mathrm{d}\Gamma = 0, \tag{5}$$

where $\delta\mathbf{d}$ and $\delta\boldsymbol{\varepsilon}$ are the virtual displacement and strain components, respectively, and $\boldsymbol{t}$ is the current traction vector acting on the surface $\boldsymbol{\Gamma}$.

After Galerkin discretization $(\Omega \approx \Sigma_e \Omega_e, \Gamma \approx \Sigma_e \Gamma_e)$, it is possible to write the multi-dimensional system in the following compact matrix form,

$$\Sigma_e \left[\int_{\Omega_e} \delta\mathbf{d}^{\mathrm{T}} \rho \ddot{\mathbf{d}}\, \mathrm{d}\Omega_{\mathrm{e}} + \int_{\Omega_e} (\mathbf{Bd})^{\mathrm{T}} \sigma \mathrm{d}\Omega_{\mathrm{e}} - \int_{\Gamma_e} \delta\mathbf{d}^{\mathrm{T}} \mathbf{t} \mathrm{d}\Gamma_{\mathrm{e}} \right] = 0, \tag{6}$$

in which **B** is a matrix containing the derivatives of the shape functions, as described in [Zienkiewicz et al., 2013]. The semi-discrete system obtained can then be discretized in time by using the α-method [Zienkiewicz et al., 2014]. This yields a non-linear system of equations:

$$\mathbf{M}\ddot{\mathbf{d}}_{\mathrm{n+1}} + \mathbf{S}(\mathbf{d}_{\mathrm{n+1}}) - \mathbf{T}_{\mathrm{n+1}} = 0, \tag{7}$$

where $\mathbf{d}_{\mathrm{n+1}}$ is the vector of unknown nodal displacements at time n+1, **M** is the mass matrix, **S** is the internal force (non-linearized) vector and $\mathbf{T}_{\mathrm{n+1}}$ is the external forces vector. The system solution is sought by employing the Newton-Raphson method, as described in [Bonet et al., 2010]. In this solution procedure the stiffness matrix, **K**, is computed as derivative of the residual of the previous system of equations with respect to the displacement **d.**

2.3. Contact mechanics algorithm

Contact mechanics problems are non-linear in nature, since contact forces, displacements and points of contact are unknowns at the interface during collision between two bodies. The contact algorithm used in this study is derived from the methodology by Doghri et al [Doghri et al., 1998]. For a more detailed explanation on contact procedure see the above-mentioned reference work.

A frictionless node-to-surface contact procedure based on the penalty method is employed where the nodes at lower surface of the graft are designated as slave nodes. Figure 3 illustrates the contact procedure for a single slave node of the graft, which is localized by the position vector x_s during the contact occurs, by its projection x_p on the corneal master surface. The quadrilateral element of the master surface is divided into four triangular facets by means of a temporary centre node '0', such that each master triangular facet has 3 nodes; 0, 1, 2. The coordinates of the temporary centre node are defined by:

$$x_0 = \frac{1}{4}\sum_{i=1}^{4} x_i \,, \tag{8}$$

The tangential edge vectors e_1 and e_2 are given by:

$$e_1 = x_1 - x_0 , \; e_2 = x_2 - x_0 \,, \tag{9}$$

The normal of the triangular facet is defined as:

$$n^{\Delta} = e_1 \times e_2 \,. \tag{10}$$

For each corner node (belonging to the quadrilateral element) the average normal is calculated by considering the normal of triangular facets connected to the node. The normal at the temporary central node of the quadrilateral element n_o is calculated by averaging the normal at the corner nodes, i.e,

$$n_0 \left| n_0 \right| = \frac{1}{4} \sum_{i=1}^{4} n_i \quad . \tag{11}$$

The initial step of the contact procedure is to project the slave node x_s along the calculated facet normal n^{Δ} onto the master surface (Figure 3(a)). This identifies the projected point x_p, lying within the triangular facet, where the contact actually occurs. In order to check the location of the projected point x_p, a natural coordinate system ξ is employed (see Figure 3(c)). The natural coordinates of the projection point are calculated from the edge vectors, dual basis vectors and normal of the facet. The dual basis vectors are calculated as:

$$w_1 = n^{\Delta} \times e_1, w_2 = n^{\Delta} \times e_2 \quad , \tag{12}$$

The natural coordinates of the projected point x_p are defined as:

$$\xi_{1p} = \frac{w_2.(x_s - x_0)}{w_2.e_1} \quad , \xi_{2p} = \frac{w_1.(x_s - x_0)}{w_1.e_2} \quad , \tag{13}$$

It is worth noticing that the projected point x_p lies within the triangular facet domain only if the natural coordinates ξ_{1p}, ξ_{2p} and their sum are in the range between 0 and 1. The coordinates of the projected point x_p are linearly interpolated by using the finite element shape functions N_i

$$x_p = \sum_{i=0}^{2} N_i x_i \, , \tag{14}$$

where

$$N_0 = 1 - \xi_{1p} - \xi_{2p}, N_1 = \xi_{1p}, N_2 = \xi_{2p} \, .$$

Every time the slave node changes position, the projected or contact point is re-calculated for each iteration of the algorithm.

The second contact step is to measure the gap vector g_i between the coordinate of the slave node and projected point, in order to check if the points are actually in contact. This gap vector is calculated along the interpolated normal n_p at the projection point on the triangular facet, which is given by

$$n_p \left| n_p \right| = \sum_{i=0}^{2} N_i n_i, \tag{15}$$

$$g = x_s - x_p, \tag{16}$$

$$g_i = g.n_p. \tag{17}$$

The gap vector, g_i, refers to the following impenetrability conditions:

$g_i < 0$	penetration;	(18)
$g_i = 0$	perfect contact;	(19)
$g_i > 0$	no contact.	(20)

Penalty constraints are applied to prevent the violation of impenetrability condition in order to satisfy the conditions (17) and (18). This is carried out by means of penalty parameter,ε, which is imposed in the contact stiffness matrix and contact force vector in order to avoid penetration.

This penalty parameter depends on the amount of penetration of the slave body into the master body. A higher value of penalty parameter decreases the amount of penetration of slave body into the master body. However, very large values of penalty parameter may lead to numerical instabilities.

In order to solve the non-linear system of contact equations, Newton-Raphson method is employed to linearize the equations at the region of contact, and iterations are performed to obtain the solution. The linearization procedure for the finite element contact formulation can be found in [Laursen et al., 1993].

The contact force f of the slave node at the contact point is defined as

$$f = \varepsilon g_i . \tag{21}$$

Since the two bodies are flexible, an equal and opposite contact force f at the master triangular facet nodes (0,1,2), are distributed based on the shape function of the corresponding nodes at the contact region, in order to impose equilibrium conditions. Therefore, the residual contact force vector matrix at contact region, $\mathbf{R_c}$ is given as:

$$\mathbf{R_c} = \left[N_0 f^T N_1 f^T N_2 f^T - f^T \right] . \tag{22}$$

The contact stiffness matrix $\mathbf{K_c}$ is defined at the point of contact between slave and master bodies as:

$$\mathbf{K_c} = \begin{bmatrix} N_0^2 m & N_0 N_1 m & N_0 N_2 m & -N_0 m \\ N_0 N_1 m & N_1^2 m & N_1 N_2 m & -N_1 m \\ N_0 N_2 m & N_1 N_2 m & N_2^2 m & -N_2 m \\ -N_0 m & -N_1 m & -N_2 m & m \end{bmatrix}, \tag{23}$$

where m is 3 x 3 matrix given by:

$$m = \varepsilon n_p n_p^T . \tag{24}$$

Finally, the derived contact stiffness matrix $\mathbf{K}_c$ and contact residual force $\mathbf{R}_c$ are added to the stiffness matrix and external force vector, respectively,

$$\mathbf{K}' = \mathbf{K} + \mathbf{K_C}, \mathbf{T}' = \mathbf{T} + \mathbf{R_C} . \tag{25}$$

The procedure developed by the authors is then applied to a benchmark problem for verification.

3. Results and discussion

3.1. Model verification: bending of plates over a cylinder

Before simulating the keratoplasty procedure, the proposed non-linear finite element contact model is tested by employing a typical contact mechanics benchmark problem: "bending of two plates over a cylinder". The computational domain is depicted in Figure 4(a)(left). Simulation parameters and boundary conditions of this problem can be found in the reference [Kopačka et al., 2015]. Due to symmetry of the stress and displacement fields, only one-eighth of the geometry is considered. The material properties of the elastic plates and cylinder are as follows: Young's Modulus, E = 2.1 $\times 10^5$ MPa, Poisson ratio, υ = 0.36. The plates are loaded with a uniform surface traction of 22.5 MPa in 'y' direction. It should be noticed that the benchmark problem has employed three dimensional second-order serendipity elements while the present model has used linear hexahedron elements to discretise the geometry. A penalty parameter ε = 5 $\times 10^5$ N/mm is selected to impose the impenetrability conditions in order to prevent the penetration of plates into the cylinder. This way the plates bend under the influence of the uniform pressure load. The distribution of σ_{yy} contours of the deformed plates over the cylinder are shown in Figure 4(a)(right). The contact pressure on the plate at z = 102.07 mm is within the range of values available from the literature (Figure 4(b)). The discrepancies between the present and the reference studies can be attributed to the variability in the discretised element used and difference in contact algorithm employed.

3.2. Dynamics of the impact between cornea and graft

In this section the dynamics of endothelial keratoplasty procedure is numerically reproduced and analysed. For this case, a time step equal to $\Delta t = 5 \times 10^{-6}$ seconds is used whilst the graft Young's Modulus is set equal to 0.3 MPa. The thickness and stiffness of cornea are considered to be the same throughout the study. The bubble pressure load is applied to the graft and gradually increased each time step up to a prescribed maximum pressure of P_{max} = 3.0 mmHg, in order to complete the attachment of the two bodies. Figure 5 depicts, at different time stages, the cornea and graft before and during the impact. At the initial time, the distance between centres of graft and cornea is equal to 0.65 mm.

The first contact occurs when the circumferential corners of the graft hit the cornea after 0.0001 seconds. At this point contact forces are exerted on the graft corners. As a consequence, stress intensity rises on the graft corners as well as on the corneal body surface, while the core regions of the graft undergo deformation (measured in terms of displacement with respect to the reference configuration) due to inertia and increase in pressure load. The graft completely attaches to the cornea after approximately 0.02 seconds. Since then, the effect of the impact is more prominent in the central region of the cornea, where higher stress is recorded. This may be caused by the higher load acting on the central region of the graft.

Figure 6(a,b) shows, for graft and cornea, the displacement magnitude (module) with respect to the reference configuration (configuration before the impact) and VM stress intensity after the complete attachment. The displacement is plotted for cornea and graft corresponding midsections with respect to y axis, whilst VM stress intensity is plotted at master and slave surfaces. The cornea exhibits a maximum displacement of 0.005 mm, whilst the graft attains a more pronounced displacement, with a maximum value of 0.6

mm. It is worth mentioning that the structural deformation (measured in terms of displacement with respect to the reference configuration) of the graft depends on several factors such as the stiffness and thickness of the material employed, bubble pressure and corneal stiffness. The maximum VM stress intensity values of graft and cornea are 0.015N/mm^2 and 0.0176 N/mm^2, respectively.

In order to analyse the contact force on the graft during the endothelial keratoplasty, the mean contact force on the slave nodes lying on the circumference of the graft (red thick line) is plotted against time in Figure 6(c). The recorded force rises with time, presenting also a high-frequency oscillatory behaviour due to non-linearity involved in the contact mechanics problem at the corneal-graft interface.

It is worth mentioning that the mean contact force also depends on the parameter which guarantees the impenetrability condition during the contact. The choice of the penalty parameter is based on trial and error method and it depends on various factors, like bubble pressure load, graft stiffness and thickness. The penalty parameters used for the cases with different bubble pressure load conditions and graft's Young's Modulus values, are reported in Table 1. It is shown that, for imposing the impenetrability condition, a higher penalty parameter is required for larger bubble pressure load and Young's Modulus.

3.3. Effect of graft stiffness on corneal biomechanics

The stiffness of the graft may vary during the donor graft preparation, depending on the methods employed and experience of the ophthalmologist. Moreover, the structural properties of graft depend on the donor age, gender and storage time. In this section, three different Young's Moduluses (E= 0.1, 0.2, 0.3 MPa) are considered for the graft. This allows analysing the effects of the graft stiffness on the contact mechanics. The maximum bubble pressure load, P_{max}, to attain during the complete expansion of bubble, is set as 3.0 mmHg. Figure 7(a-c) depicts the Von Mises stress intensity plotted at the central section of master surface of cornea and slave surface of graft while the displacement is plotted at the central -section of mid-surface of graft and cornea. For lower values of E, the graft exhibits a more deformable behaviour and consequently, the impact of the graft induces larger stress and strain on the cornea. The curve corresponding to case E = 0.2 MPa (green dashed dot line) lies between the other two cases. Figure 7(d) shows that a stiffer graft involves a higher contact force. On the contrary, if the graft is able to deform more, the smaller reaction-contact force between the two body forces favour penetration.

3.4. Effect of bubble pressure load on corneal biomechanics

In endothelial keratoplasty surgery, the bubble pressure load plays a fundamental role for the complete adhesion of the graft. It is indeed possible to experience a partial attachment due to an insufficient bubble expansion. Moreover, if the graft stiffness is higher, an additional pressure load, through expanding the bubble, is required to deform the graft for the complete attachment. At the same time, a very large pressure load can lead to abnormal stress on the contact surface, involving potentially dangerous consequences on the health of the corneal cells. In order to elucidate the corneal structural response dependency on pressure, three different values of bubble pressure loads, (1.5, 2.3, 3.0 mmHg) are considered. The Young's Modulus of the graft is set E=0.1 MPa. Simulation results show that, for larger bubble pressure loads (2.3 mmHg, 3 mmHg), the graft and cornea sustain higher stress (0.03-.032 MPa) after the attachment, as shown in Figure 8 (a-c) (green dashed dot line, blue dashed double dot line). The cornea deforms more when the graft is under larger loads (Figure 8(c)). As the bubble pressure load increases, the mean contact force on the graft becomes higher as shown in Figure 8(d). It is also important to mention that the time required for the graft to attach is significantly smaller (0.017-0.020 seconds) for larger pressure loads (2.3-3.0 mmHg).

3.5. Effect of graft thickness on corneal biomechanics

The thickness and diameter of the graft depends on the technique adopted (DMAEK, DSAEK). Based on the patient's need, ophthalmologists usually develop a donor graft within the thickness range: 50-120 µm. Here the influence of graft thickness (50, 80, 100 and 120 µm) on corneal deformation (evaluated in displacement module with respect to the reference configuration) and stress intensity is investigated (see Figure 9(a-c)). The maximum bubble pressure load is set P_{max}=2.5 mmHg and Young's Modulus E=0.2 MPa. The graft stress recorded are higher at the central regions for thickness of 50 µm (thick red line) and 80 µm (green dashed double dot line) than in the case of 100 µm (blue dashed dot line) and 120 µm (pink dashed line). This is due to the fact that deformation decreases for larger graft thickness.

For the same applied bubble load, a graft with thickness 50 µm has a higher acceleration than the thicker ones and consequently the impact will produce larger corneal deformation and stress, as shown in Figure 9 (thick red line). On the contrary, for a higher graft thickness (100 µm and 120 µm), the deformation is more uniform and it occurs in a more controlled manner. It is important to notice from Figure 9(d) that the mean contact force developed at the contact surface increases with the graft thickness.

4. Conclusions

In the present work, endothelial keratoplasty, a corneal transplantation technique, is computationally modelled by employing a hyper-elastic finite element framework. The automated air bubble technique is also numerically reproduced in order to induce the graft attachment to the cornea. Since this surgical technique involves contact between graft and cornea, a penalty-based node-to-surface contact model is integrated into the hyper-elastic finite element model.

Displacement and VM stress analysis show that the changes in geometrical and material properties of graft have significant effects on biomechanical behaviour of the cornea. A lower stiffness and thickness of the graft induce higher corneal stress intensity and deformation during the impact. This is more evident for high bubble pressure loads. Undoubtedly, the air bubble pressure load condition plays a fundamental role in the graft-cornea attachment.

Simulation results can provide a valuable insight for a more efficient endothelial keratoplasty surgery design, accounting for geometric, material and air bubble pressure conditions. The current study serves as a foundation for the future work which involves the effect of Aqueous Humor (AH) flow on the graft attachment with cornea. In this way, the detachment sites of graft can be analysed which provides some valuable information for the surgeons in order to reduce the post-operative complications.

Acknowledgements

Alessandro Mauro also gratefully acknowledges the local program of the University of Napoli "Parthenope" for the support to individual research.

Conflict of interest statement

The authors have no conflict of interest in the materials discussed in this work.

5. References

1. Bonet, J., Wood, R.D., (2010) Nonlinear continuum mechanics for finite element analysis. Second edition. Cambridge University Press.

2. Canovetti, A., Rossi, F., Rossi, M., Menabuoni, L., Malandrini, A., Pini, R., Ferrara, P. (2018) Anvil-profiled penetrating keratoplasty: load resistance evaluation, Biomechanics and Modeling in Mechanobiology. doi: 10.1007/s10237-018-1083-y
3. Doghri, I., Muller, A., Taylor, R.L. (1998) A general three-dimensional contact procedure for implicit finite element codes, Engineering Computations. 15(2), 233-259. https://doi.org/10.1108/02644409810202639
4. Fraldi, M., Cutolo, A., Esposito, L., Guarracino, F. (2011) The role of viscoelasticity and stress gradients on the outcome of conductive keratoplasty, Biomechanics and Modeling in Mechanobiology. 10(3), 397-412. doi: 10.1007/s10237-010-0242-6
5. Gormsen, A., Ivarsen, A., Hjortdal, J. (2018) Retrospective Single-Center Registry Study on Graft Thickness 1 Year After Descemet Stripping Automated Endothelial Keratoplasty. Cornea. doi: 10.1097/ICO.0000000000001793
6. Holzapfel G.A., (2000) Non-linear solid mechanics: a continuum approach for engineering. Chichester; New York:Wiley, c2000.
7. Khan, N.H., Shiakolas, P.S. (2016) Finite Element Analysis of Descemet's Stripping Automated Endothelial Keratoplasty (DSAEK) Surgery Allograft to Predict Endothelial Cell Loss, Current Eye Research. 42(1), 32-40. https://doi.org/10.3109/02713683.2016.1151052
8. Kopačka, J., Gabriel, D., Plešek, J., Ulbin, M., (2015) Assessment of methods for computing the closest point projection, penetration, and gap functions in contact searching problems, International Journal for Numerical Methods in Engineering. 105(11), 803-833. https://doi.org/10.1002/nme.4994

9. Lago, M.A., Rupérez, M.J., F.Martínez-Martínez, F., Monserrat, C., Larra, E., Güell, J.L., Peris-Martínez,C., (2010) A new methodology for the in-vivo estimation of the elastic constants that characterize the patient-specific biomechanical behaviour of the human cornea. Journal of Biomechanics. 48(1), 38-43. doi: 10.1016/j.jbiomech.2014.11.009
10. Last, J.A., Liliensiek, S.J., Nealey,P.F., Murphyaa, C.J. (2009) Determining the mechanical properties of human corneal basement membranes with Atomic Force Microscopy. Journal of Structural Biology. doi: 10.1016/j.jsb.2009.03.012
11. Laursen, T.A., Simo, J.C. (1993) A continuum-based finite element formulation for the implicit solution of multibody, large deformation-frictional contact problems, International Journal for Numerical Methods in Engineering. 36(20), 3451-3485. https://doi.org/10.1002/nme.1620362005
12. Mauro, A., Massarotti, N., Salahudeen, M,, Una, I.R., Romano, M.R., Romano, V., (2018) A novel patient-oriented numerical procedure for glaucoma drainage devices, International Journal for Numerical Methods in Biomedical Engineering. 34(12), e3141. https://doi.org/10.1007/s11517-018-1813-4.
13. Mauro, A., Massarotti, N., Salahudeen, M., Romano, M.R., Romano, V., Nithiarasu, P., (2018) A generalised porous medium approach to study thermo-fluid dynamics in human eyes, Medical & Biological Engineering & Computing. 56(10),1823-1839. https://doi.org/10.1002/cnm.3141.
14. Mauro, A., Romano, M.R., Romano, V., Nithiarasu, P (2018) Suprachoroidal shunts for treatment of glaucoma: a comparison based on numerical simulations, International Journal of Numerical Methods for Heat & Fluid Flow, 28(2), 297-314. doi:10.1108/HFF-12-2016-0508.

15. Mauro, A., Massarotti, N., Salahudeen, M., Cuomo, F., Costagliola, C., Ambrosone, L., Romano, M.R., (2018) Design of a novel heating device for infusion fluids in vitrectomy, Applied Thermal Engineering, 128, 625-636. doi:10.1016/j.applthermaleng.2017.08.027.

16. Montanino, A., Angelillo, M., Pandolfi, A., (2018) Modelling with a mesh free approach the cornea-aqueous humor interaction during the air puff test. Journal of the Mechanical Behavior of Biomedical Materials. 77, 205-216. doi: 10.1016/j.jmbbm.2017.05.042

17. Moshirfar, M., Imbornoni, L.M., Muthappan, V., Williams, L., Khalifa, Y.M., Jarstad, A., Sikder, S. (2014) In vitro pilot analysis of uniformity, circularity, and concentricity of DSAEK donor endothelial grafts prepared by a microkeratome. Cornea. 33(2), 191-6. doi: 10.1097/ICO.0000000000000031

18. Nguyen, T.D., Boyce, B.L. (2011) An inverse finite element method for determining the anisotropic properties of the cornea. Biomechanics and Modeling in Mechanobiology. 10(3), 323-337. doi: 10.1007/s10237-010-0237-3

19. Pandolfi, A., Manganiello, F. (2006) A model for the human cornea: constitutive formulation and numerical analysis. Biomechanics and Modeling in Mechanobiology. 5(4), 237-246. https://doi.org/10.1007/s10237-005-0014-x

20. Parekh, M., Leon. P., Ruzza, A., Borroni, D., Ferrari, S., Ponzin, D., Romano, V., (2018) Graft detachment and rebubbling rate in Descemet membrane endothelial keratoplasty. Survey of Ophthalmology. 63(2), 245-250. doi:10.1016/j.survophthal.2017.07.003

21. Parekh, M,, Ruzza, A., Kaye, A., Steger, B., Kaye, S.B., Romano, V., (2018) Descemet Membrane Endothelial Keratoplasty-Complication and management of a single case for tissue preparation and graft size linked to post-op

descemetorhexis disparity. American Journal of Ophthalmology Case Reports. 12, 65-67. doi: 10.1016/j.ajoc.2018.09.003

22. Shih, P., Huang, C., Huang, T., Lin, H., Yen, J., Wang, I., Cao, H., Shih, W., Dai, C (2017) Estimation of the Corneal Young's Modulus In Vivo Based on a Fluid-Filled Spherical-Shell Model with Scheimpflug Imaging. Journal of Ophthalmology. 5410143. https://doi.org/10.1155/2017/5410143

23. Sinha, R.A., Dupps, W.J. Jr., (2009) Effects of altered corneal stiffness on native and postoperative LASIK corneal biomechanical behavior: A whole-eye finite element analysis.Journal of Refractive Surgery. 25(10), 875-87. doi: 10.3928/1081597X-20090917-09

24. Stuart, A.J., Romano. V., Virgili. G., Shortt. A.J., (2018) Descemet's membrane endothelial keratoplasty (DMEK) versus Descemet's stripping automated endothelial keratoplasty (DSAEK) for corneal endothelial failure. Cochrane Database of Systematic Reviews 6, CD012097. doi:10.1002/14651858.CD012097.pub2

25. Studer, H., Larrea, X., Riedwyl, H., Buchler, P., (2010) Biomechanical model of human cornea based on stromal microstructure. Journal of Biomechanics. 43, 836-842. doi: 10.1016/j.jbiomech.2009.11.021

26. Tan, D.T., Dart. J.K., Holland. E.J., Kinoshita. S., (2012) Corneal transplantation. Lancet 79(9827), 1749-61. doi: 10.1016/S0140-6736(12)60437-1.

27. Whitford, C., Studer, H., Boote, C., Meek, K.M., Elsheikh, A., (2015) Biomechanical model of the human cornea: considering shear stiffness and regional variation of collagen anisotropy and density. Journal of the Mechanical Behavior of Biomedical Materials. 42, 76-87. doi: 10.1016/j.jmbbm.2014.11.006

28. Zienkiewicz O.C., Taylor R.L., Zhu J.Z., (2013) The finite element method: Its basis and fundamentals. Seventh Edition. Butterworths-Heinemann.

29. Zienkiewicz O.C., Taylor R.L., Fox D., (2014) The finite element method for solid and structural mechanics. Seventh Edition. Butterworths-Heinemann.

P_{max} (mmHg) / E (MPa)	1.5	2.3	3.0
0.1	0.0050 N/mm	0.0080 N/mm	0.01 N/mm
0.2	0.0055 N/mm	0.0085 N/mm	0.017 N/mm
0.3	0.0070 N/mm	0.0095 N/mm	0.025 N/mm

Table 1. Penalty parameter ε for different bubble pressure loads P_{max} and graft Young's Modulus E.

Figure captions

Fig. 1 Endothelial Keratoplasty procedure (DMAEK and DSAEK)

Fig. 2 Computational domain and boundary conditions of graft and cornea. The graft is initially positioned parallel to x and z axis, with the slave surface facing the master surface of the cornea

Fig. 3 (a) Projection of slave node x_s onto the master surface, (b) tangential vectors of triangular facet and (c) local coordinate system (ξ) of the projected point x_p

Fig. 4 (a) Plates mounted over a cylinder (left) Computational domain of the bending plates over a cylinder (right) (b) Contact pressure distribution on the plate

Fig. 5 Von Mises stress intensity plotted at (a) different time steps for the cornea and graft, (b) different time steps at central-section of the cornea and graft and (c) graft and cornea after complete attachment (left), posterior and anterior parts of the cornea after complete attachment (right)

Fig. 6 (a) Displacement at cornea (left) and graft (right), (b)VM stress at cornea (Master surface) (left) and graft (slave surface) (right) and (c) mean contact force at the slave nodes of the circumference of graft

Fig. 7 VM stress intensity at (a) graft (slave surface), (b) cornea (master surface), (c) displacement at cornea and (d) mean contact force at the slave nodes of the circumference of graft

Fig. 8 VM stress intensity at (a) graft (slave surface), (b) cornea (master surface), (c) displacement at cornea and (d) mean contact force at the slave nodes of the circumference of graft

Fig. 9 VM stress intensity at (a) graft (slave surface), (b) cornea (master surface), (c) displacement at cornea, and (d) mean contact force at the slave nodes of the circumference of graft

KERATOPLASTY PROCEDURE

Insertion of graft inside the Anterior Chamber of eye | **Insertion of Air Bubble (AB) at the centre of graft** | **Expansion of Air Bubble and attachment of graft to the cornea**

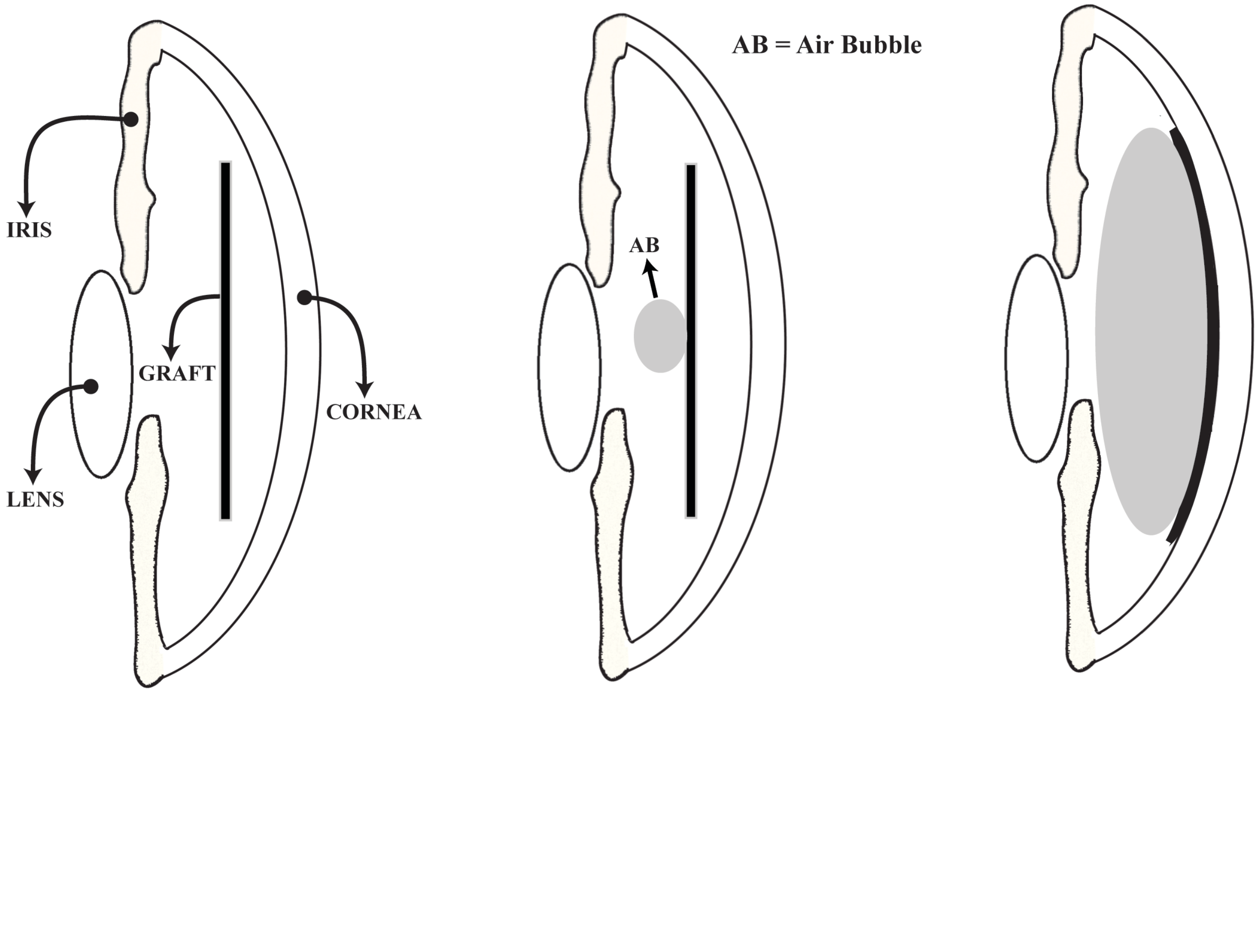

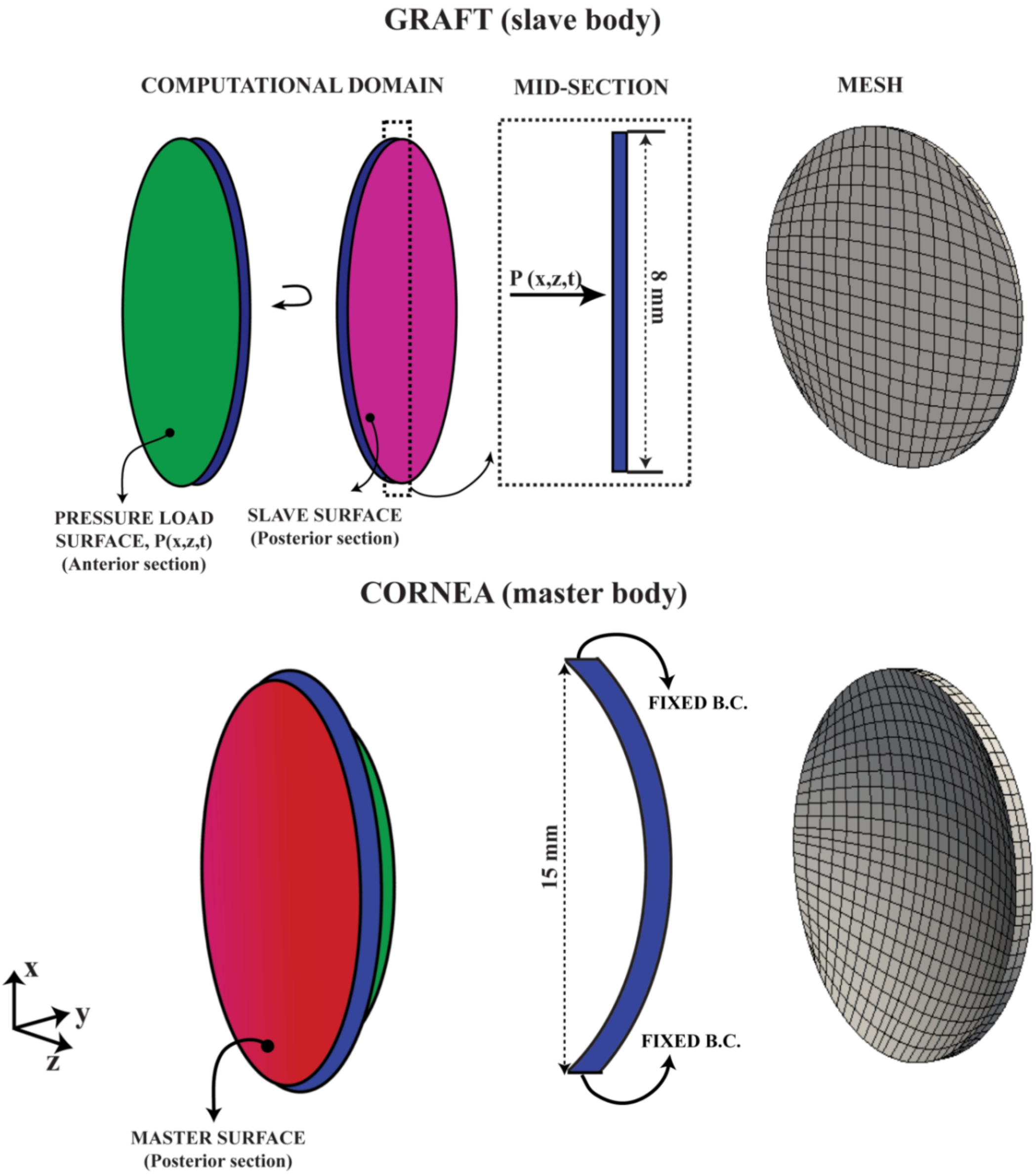

GRAFT (slave body)
COMPUTATIONAL DOMAIN
MID-SECTION
MESH
P (x,z,t)
8 mm
PRESSURE LOAD
SURFACE, P(x,z,t)
(Anterior section)
SLAVE SURFACE
(Posterior section)
CORNEA (master body)
FIXED B.C.
15 mm
FIXED B.C.
x
y
z
MASTER SURFACE
(Posterior section)

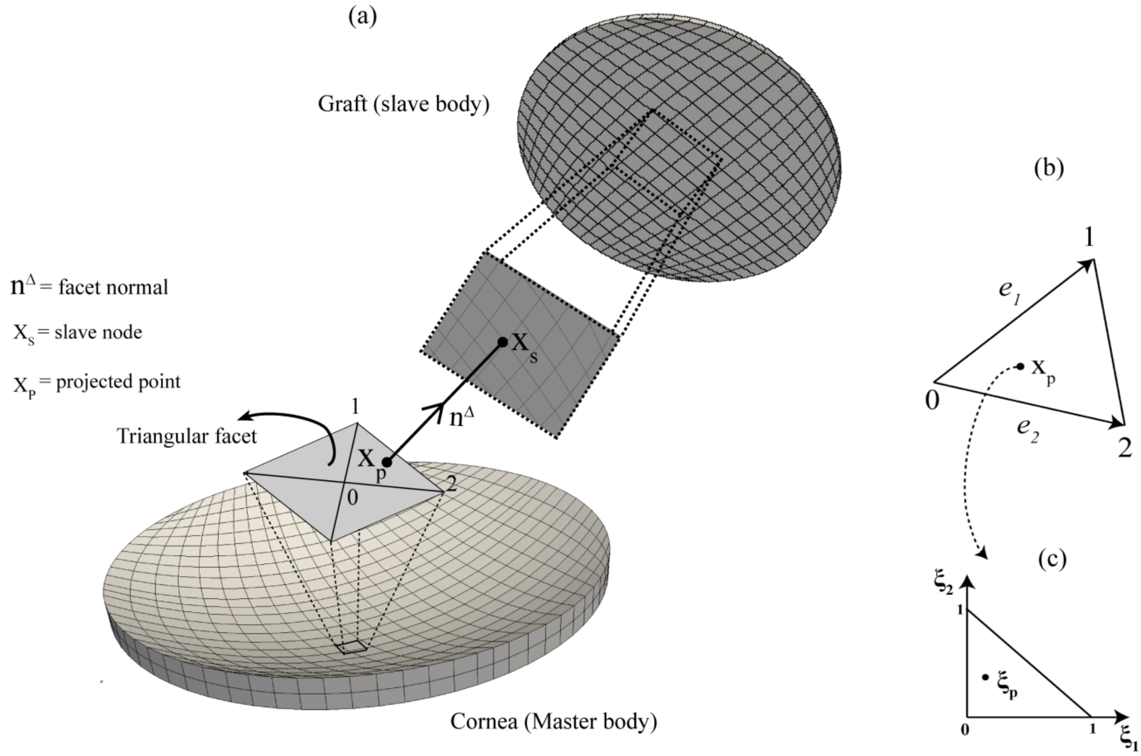
(a)
Graft (slave body)
n^{Δ} = facet normal
X_S = slave node
X_P = projected point
Triangular facet
1
X_p
0
2
n^{Δ}
X_s
Cornea (Master body)
(b)
1
e_1
x_p
0
e_2
2
(c)
ξ_2
1
ξ_p
0
1
ξ_1

(a)

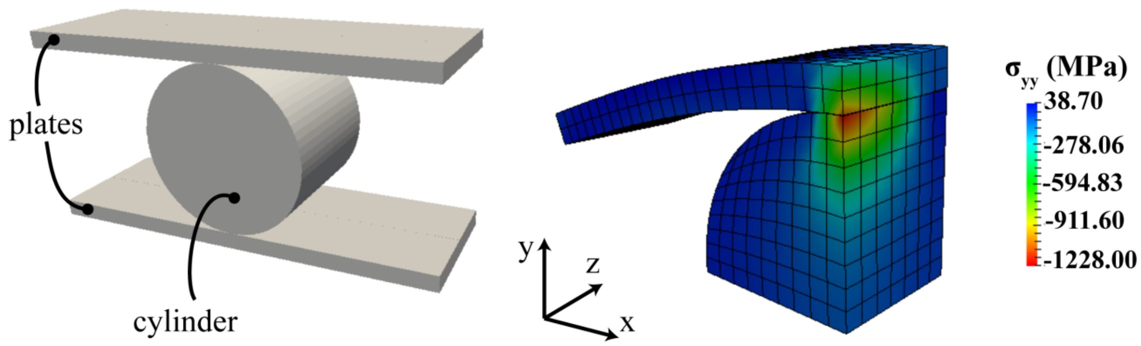
plates
cylinder
y
z
x
σyy (MPa)
38.70
-278.06
-594.83
-911.60
-1228.00

(b)

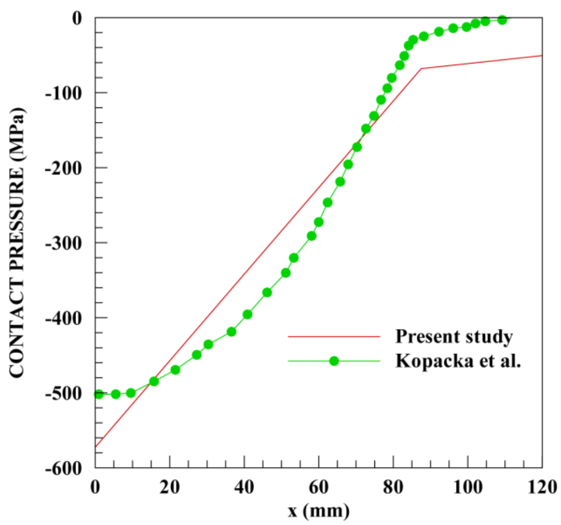
CONTACT PRESSURE (MPa)
x (mm)
Present study
Kopacka et al.
0
-100
-200
-300
-400
-500
-600
0
20
40
60
80
100
120

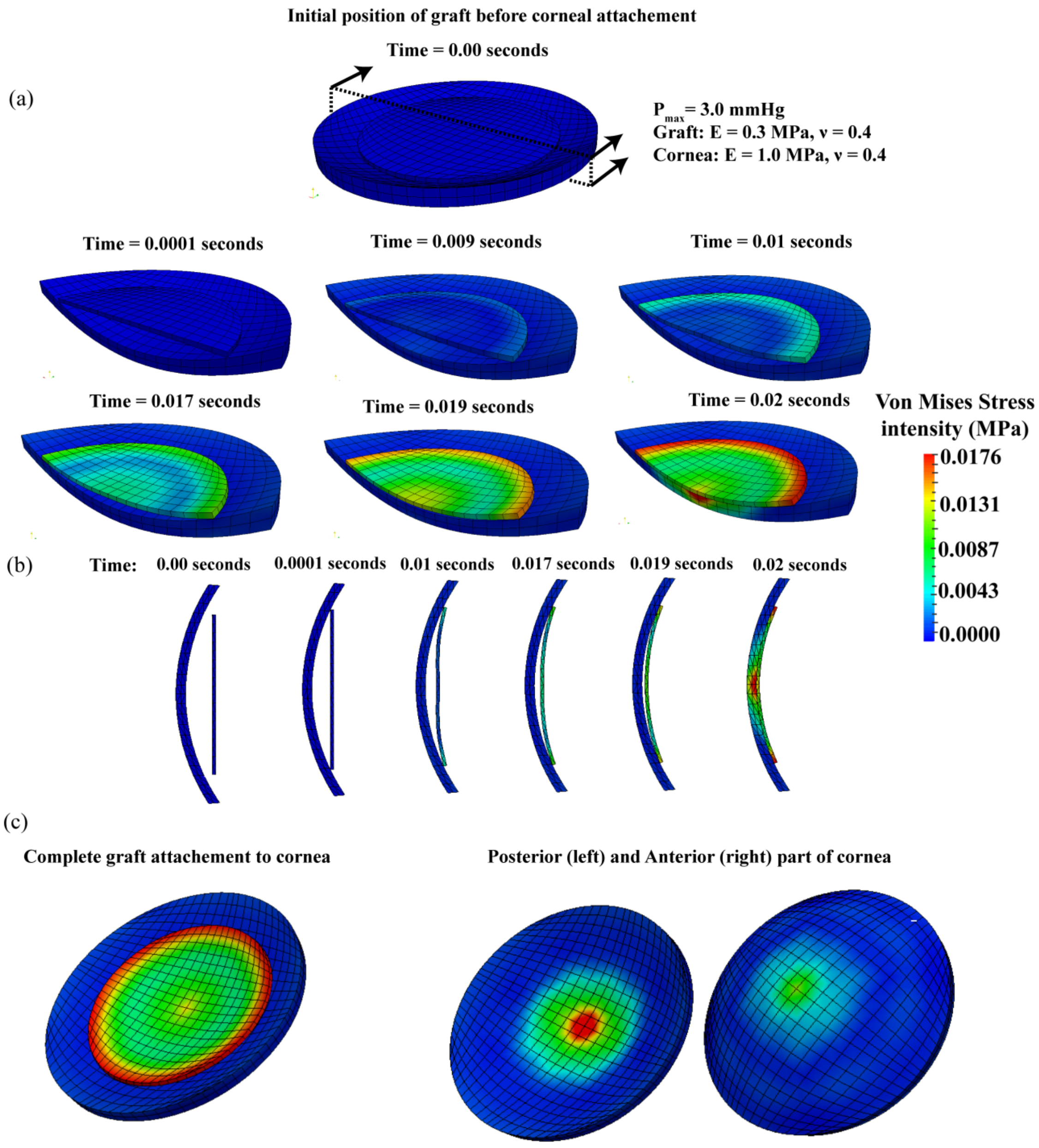

Initial position of graft before corneal attachement
Time = 0.00 seconds
(a)
P_{max} = 3.0 mmHg
Graft: E = 0.3 MPa, ν = 0.4
Cornea: E = 1.0 MPa, ν = 0.4
Time = 0.0001 seconds
Time = 0.009 seconds
Time = 0.01 seconds
Time = 0.017 seconds
Time = 0.019 seconds
Time = 0.02 seconds
Von Mises Stress intensity (MPa)
0.0176
0.0131
0.0087
0.0043
0.0000
(b)
Time: 0.00 seconds
0.0001 seconds
0.01 seconds
0.017 seconds
0.019 seconds
0.02 seconds
(c)
Complete graft attachement to cornea
Posterior (left) and Anterior (right) part of cornea

(a)

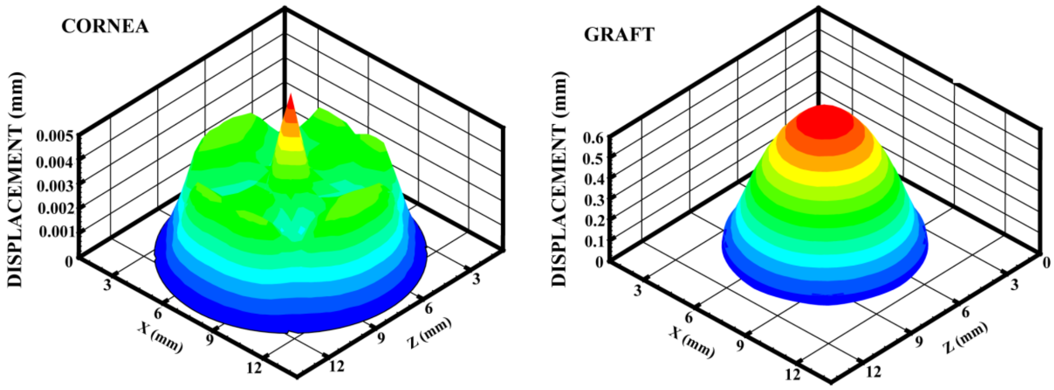
CORNEA
DISPLACEMENT (mm)
0.005
0.004
0.003
0.002
0.001
0
X (mm)
Z (mm)
3
6
9
12
GRAFT
0.6
0.5
0.4
0.3
0.2
0.1

(b)

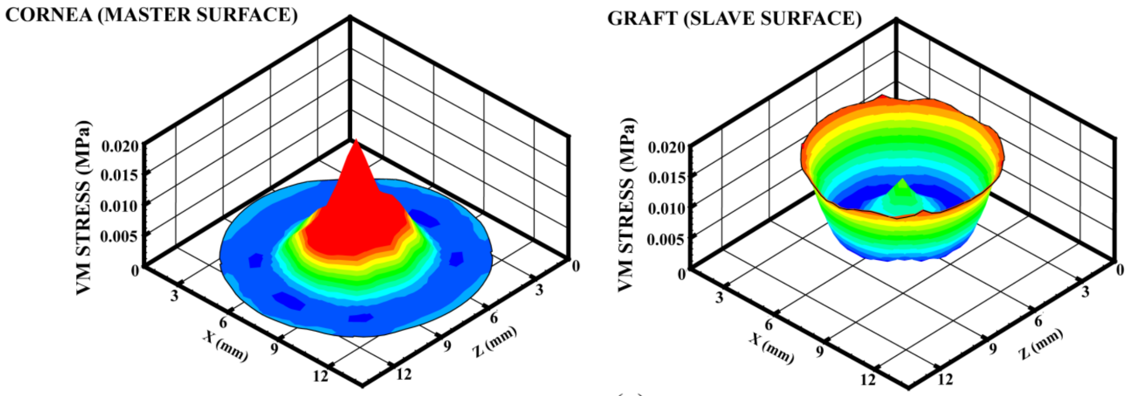
CORNEA (MASTER SURFACE)
GRAFT (SLAVE SURFACE)
VM STRESS (MPa)
0.020
0.015
0.010
0.005
0
X (mm)
Z (mm)
3
6
9
12

(c)

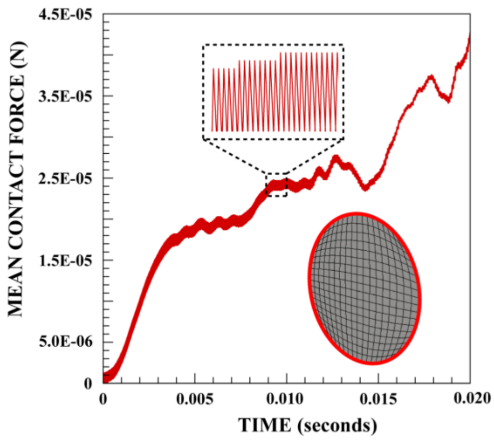
MEAN CONTACT FORCE (N)
4.5E-05
3.5E-05
2.5E-05
1.5E-05
5.0E-06
0
TIME (seconds)
0
0.005
0.010
0.015
0.020

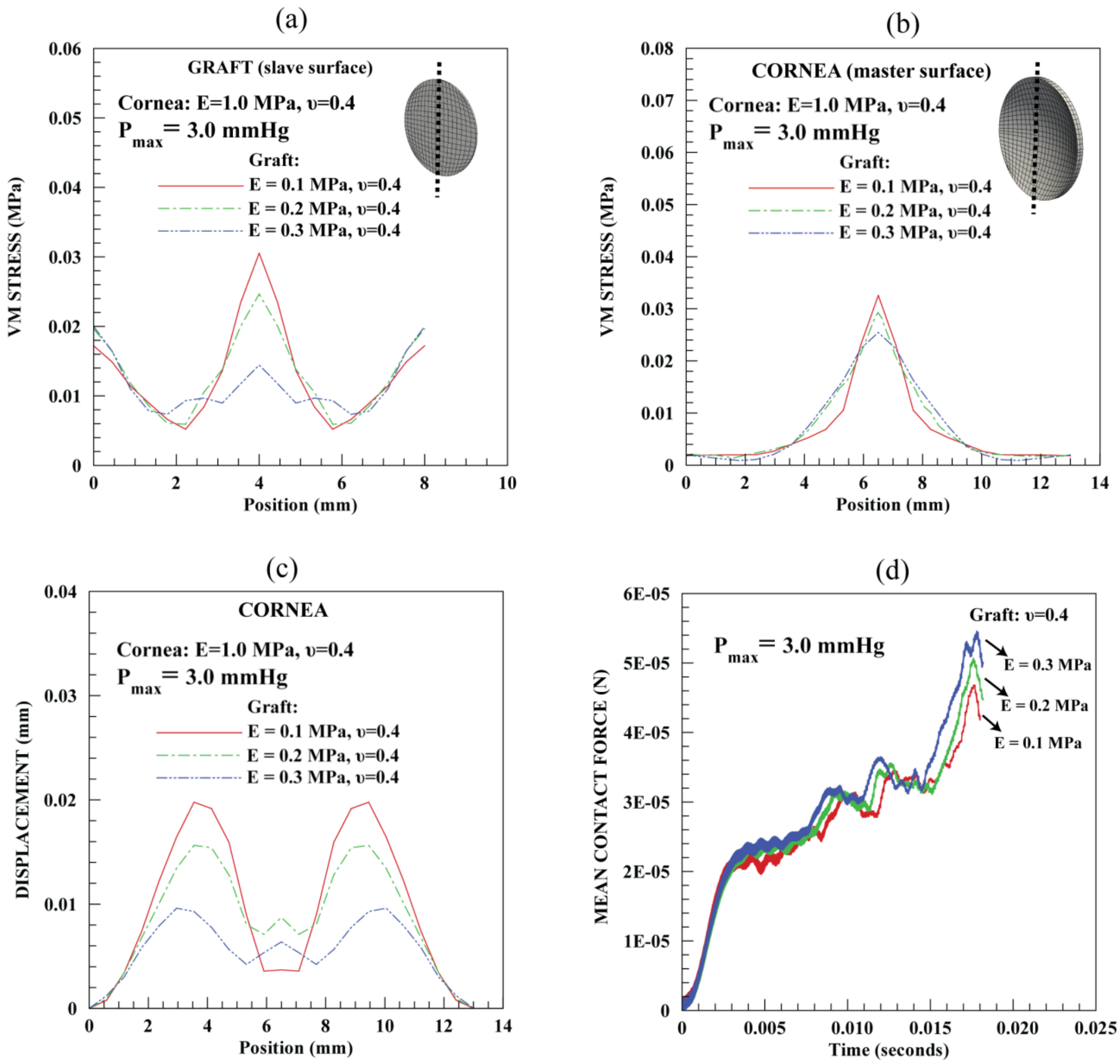
(a)
GRAFT (slave surface)
Cornea: E=1.0 MPa, υ=0.4
P max = 3.0 mmHg
Graft:
E = 0.1 MPa, υ=0.4
E = 0.2 MPa, υ=0.4
E = 0.3 MPa, υ=0.4
VM STRESS (MPa)
Position (mm)
0 0.01 0.02 0.03 0.04 0.05 0.06
0 2 4 6 8 10
(b)
CORNEA (master surface)
Cornea: E=1.0 MPa, υ=0.4
P max = 3.0 mmHg
Graft:
E = 0.1 MPa, υ=0.4
E = 0.2 MPa, υ=0.4
E = 0.3 MPa, υ=0.4
VM STRESS (MPa)
Position (mm)
0 0.01 0.02 0.03 0.04 0.05 0.06 0.07 0.08
0 2 4 6 8 10 12 14
(c)
CORNEA
Cornea: E=1.0 MPa, υ=0.4
P max = 3.0 mmHg
Graft:
E = 0.1 MPa, υ=0.4
E = 0.2 MPa, υ=0.4
E = 0.3 MPa, υ=0.4
DISPLACEMENT (mm)
Position (mm)
0 0.01 0.02 0.03 0.04
0 2 4 6 8 10 12 14
(d)
P max = 3.0 mmHg
Graft: υ=0.4
E = 0.3 MPa
E = 0.2 MPa
E = 0.1 MPa
MEAN CONTACT FORCE (N)
Time (seconds)
0 1E-05 2E-05 3E-05 4E-05 5E-05 6E-05
0 0.005 0.010 0.015 0.020 0.025

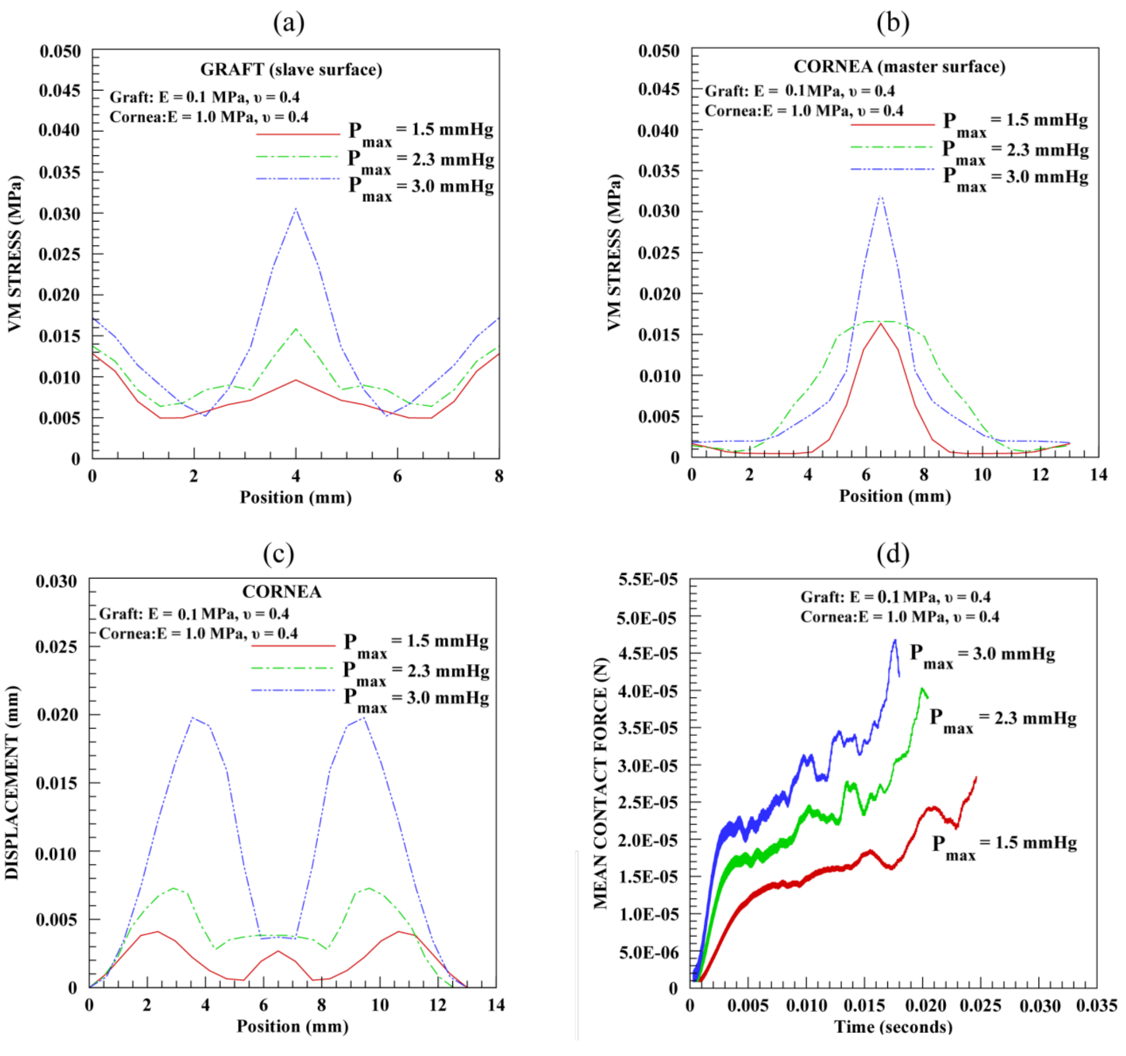

(a)
GRAFT (slave surface)
Graft: E = 0.1 MPa, υ = 0.4
Cornea:E = 1.0 MPa, υ = 0.4
P max = 1.5 mmHg
P max = 2.3 mmHg
P max = 3.0 mmHg
VM STRESS (MPa)
Position (mm)
(b)
CORNEA (master surface)
Graft: E = 0.1 MPa, υ = 0.4
Cornea:E = 1.0 MPa, υ = 0.4
P max = 1.5 mmHg
P max = 2.3 mmHg
P max = 3.0 mmHg
VM STRESS (MPa)
Position (mm)
(c)
CORNEA
Graft: E = 0.1 MPa, υ = 0.4
Cornea:E = 1.0 MPa, υ = 0.4
P max = 1.5 mmHg
P max = 2.3 mmHg
P max = 3.0 mmHg
DISPLACEMENT (mm)
Position (mm)
(d)
Graft: E = 0.1 MPa, υ = 0.4
Cornea:E = 1.0 MPa, υ = 0.4
P max = 3.0 mmHg
P max = 2.3 mmHg
P max = 1.5 mmHg
MEAN CONTACT FORCE (N)
Time (seconds)

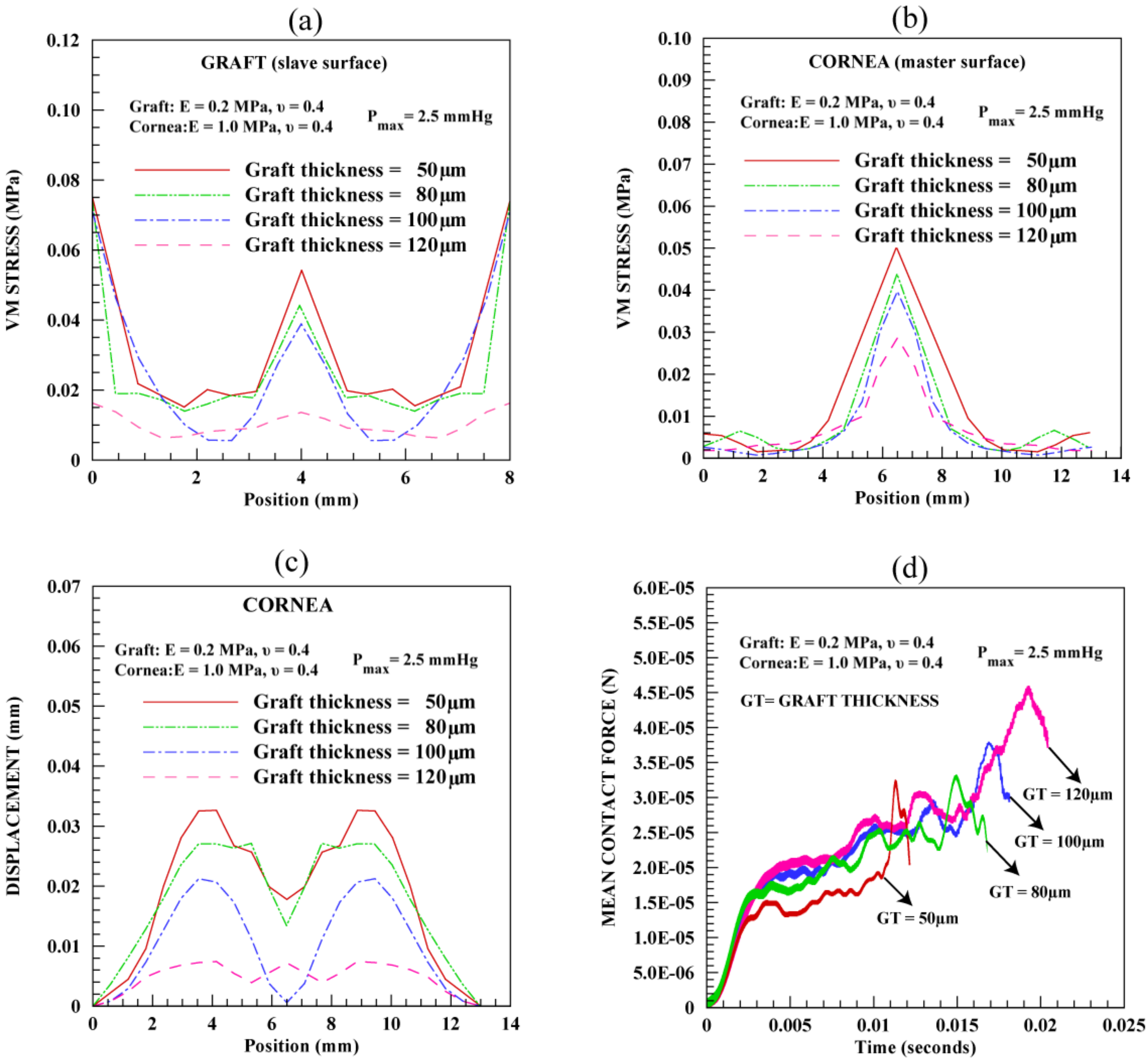
(a)
GRAFT (slave surface)
Graft: E = 0.2 MPa, υ = 0.4
Cornea:E = 1.0 MPa, υ = 0.4
P max = 2.5 mmHg
Graft thickness = 50 µm
Graft thickness = 80 µm
Graft thickness = 100 µm
Graft thickness = 120 µm
VM STRESS (MPa)
Position (mm)
(b)
CORNEA (master surface)
Graft: E = 0.2 MPa, υ = 0.4
Cornea:E = 1.0 MPa, υ = 0.4
P max = 2.5 mmHg
Graft thickness = 50 µm
Graft thickness = 80 µm
Graft thickness = 100 µm
Graft thickness = 120 µm
VM STRESS (MPa)
Position (mm)
(c)
CORNEA
Graft: E = 0.2 MPa, υ = 0.4
Cornea:E = 1.0 MPa, υ = 0.4
P max = 2.5 mmHg
Graft thickness = 50 µm
Graft thickness = 80 µm
Graft thickness = 100 µm
Graft thickness = 120 µm
DISPLACEMENT (mm)
Position (mm)
(d)
Graft: E = 0.2 MPa, υ = 0.4
Cornea:E = 1.0 MPa, υ = 0.4
P max = 2.5 mmHg
GT= GRAFT THICKNESS
GT = 120µm
GT = 100µm
GT = 80µm
GT = 50µm
MEAN CONTACT FORCE (N)
Time (seconds)